J Solid State Electrochem (2012) 16:2373–2381
DOI 10.1007/s10008-011-1613-3

ORIGINAL PAPER

Electrochemical deposition of gold at liquid–liquid interfaces studied by thin organic film-modified electrodes

Birhan Sefer · Rubin Gulaboski · Valentin Mirčeski

Received: 30 October 2011 / Revised: 27 November 2011 / Accepted: 30 November 2011 / Published online: 21 December 2011

Abstract The unique physico-chemical properties of gold nanoparticles portrayed in their chemical stability, the size-dependent electrochemistry, and the unusual optical properties make them suitable modifiers of various surfaces used in the fields of optical devices, electronics, and biosensors. In this work we present two different methods to obtain metallic gold nanoparticles at a liquid–liquid interface, and to control their growth by adjusting the experimental conditions. Decamethylferrocene (DMFC), used as an oxidizable compound dissolved in an organic solvent that is spread as a thin film on the surface of graphite electrode, serves as a redox partner to exchange electrons across the liquid–liquid interface with the other redox counter-partner $[AuCl_4]^-$ present in the conjoined water phase. The interfacial electron transfer between the DMFC and the $[AuCl_4]^-$ ions leads to deposition of metallic gold nanoparticles at the liquid–liquid interface. The structure and features of the deposited Au nanoparticles were studied by means of microscopic and voltammetric techniques. The morphology of the Au deposit depends on the concentration ratio of redox partners and both electrode and liquid–liquid interfacial potential differences. Depending on whether the Au deposit was obtained by ex situ (at open circuit potential) or by "in situ" (by cycling of the electrode potential) approach, we observed quite different effects to the ion transfer reactions probed by the thin-film electrode set-up. The possible reasons for the different behavior of the Au nanoparticles are discussed in terms of the structure and the properties of the obtained Au deposit. In separate experiments, we have demonstrated catalytic effects of the Au nanoparticles towards enhancing the electron transfer between DMFC and two aqueous redox substrates, hexacyanoferrate and hydrogen peroxide.

Keywords Metal deposition · Liquid–liquid interface · Gold nanoparticles · Thin-film electrodes

Introduction

In the last two decades, nanoscience became an important research area dealing with materials sized to an atomic level. Nanoparticles of different materials attracted considerable attention mainly due to their high potential for numerous applications in advanced technologies. The surface, electronic, and optoelectronic properties of many materials are significantly affected by the size and the nature of the nanoparticles. The specific physico-chemical features of nanoparticles make them quite suitable for designing various sensing devices, such as electrochemical and bioelectrochemical sensors. In this respect, the nanoparticles of the noble metals and various noble metal oxides are seen as crucial factors in improving the sensing properties of many electrodes towards important substrates. Numerous chemical methods have been developed for preparation of metal particles in a single phase [1–3] including those for controlling their surface morphology and properties [4–6]. Among a variety of experimental methodologies, electrochemistry provides numerous possibilities for preparation and the size control of the metal nanoparticles, as demonstrated, for

For the special issue dedicated to the 75th birthday of Dr. Nina F. Zakharchuk.

B. Sefer · R. Gulaboski · V. Mirčeski
Institute of Chemistry, Faculty of Natural Sciences and Mathematics, "Ss Cyril and Methodius" University, PO Box 162, 1000 Skopje, Republic of Macedonia

R. Gulaboski · V. Mirčeski (✉)
Department of Chemistry, University "Goce Delčev", Štip, Republic of Macedonia
e-mail: valentin@pmf.ukim.mk

instance, by Reetz and Halbig [7]. Besides single-phase preparation methods, particularly attractive are those reporting metal deposition at the interface between two immiscible liquids [4, 8–10], most frequently, between two immiscible electrolyte solutions (ITIES) [11–17].

The liquid interface is a unique environment separating two liquids having quite different physical and chemical properties [18]. Due to its molecular smoothness, the liquid–liquid interface is seen as important environment for fundamental study of the metal deposition at a defect-free boundary. On the other hand, the liquid interface enriched with metal nanoparticles is of exceptional importance for catalysis and sensor technologies. A four-electrode set-up has been frequently applied to study the deposition of metal particles at ITIES, as in the case of silver and copper [19] deposition. Cheng and Schiffrin [20] reported formation of gold nanoparticles at ITIES, while palladium deposition has been studied by Johans et al. [21–23]. Dryfe et al. [24, 25] studied the role of interfacial potential on the deposition of platinum and palladium at a bare and templated liquid interface, suggesting strategy for morphological characterization of the metal particles. Samec et al. [26] demonstrated that Pt deposition at water/1,2-dichloroethane is controlled by the interfacial kinetics, while the activity of the Pt particles at the interface does not differ significantly from that of the bulk metal phase. In addition, a procedure for preparation of polymer-coated metal particles at ITIES was recently published [27]. Scholz et al. [16, 28] developed an electrolles methodology for silver deposition at the ITIES, while tuning the morphology of the metal deposit from silver nanowires to a smooth silver film. Recently, we reported the first usage of thin organic film-modified electrodes for preparation of Ag nanoparticles at ITIES, and we studied their catalytic properties toward various biosubstrates [29, 30]. Song et al. [31] used similar electrode set-up to study the transfer of $[AuCl_4]^-$ from water into toluene, followed by an electrode reduction and formation of a highly porous metallic gold on the electrode surface, rather than formation of individual Au nanoparticles at the liquid–liquid interface.

In the present study, we demonstrate that the thin organic film-modified electrodes can be further effectively exploited for deposition of metallic gold nanoparticles at the water/nitrobenzene (w/nb) interface. The electrode set-up (Fig. 1) consists of a black graphite electrode, covered with a thin film of nitrobenzene, containing decamethylferrocene (DMFC) as a lipophilic redox active compound and a suitable organic electrolyte. The modified electrode is immersed in an aqueous electrolyte solution containing $[AuCl_4]^-$(w) ions to prompt spontaneous heterogeneous redox reaction with DMFC(nb), yielding a gold deposit at the liquid interface. Such electrode assembly, together with the three-phase electrodes with a droplet configuration [32], is highly sensitive to the charge transfer phenomena at the liquid interface, providing a basis for studying thermodynamics of ion transfers [33, 34] as well as the kinetics of ion [35, 36] and electron transfer reactions [37, 38]. Hence, when the heterogeneous electron transfer reaction occurring at the liquid interface results in formation of a metal deposit at the interface, it is expected that the electrochemical response of the modified electrode will be strongly affected, which is the basis of the present experimental work.

Two different strategies for preparation of Au deposit have been applied: (1) open circuit deposition protocol (ex situ), conducted by conditioning the modified electrode in an aqueous solution containing $[AuCl_4]_{(W)}^-$ ions, and (2) electrochemical deposition protocol (in situ), conducted by potential cycling and repetitive turnover of the redox couple (DMFC(nb)/$DMFC^+$(nb)) in the thin film. Besides voltammetry, the gold particles have been evidenced by microscopic techniques. We have also demonstrated the catalytic activity of gold deposit toward the electron transfer reactions with various substrates at the liquid interface.

Experimental section

All chemicals used were of analytical grade purity. DMFC was purchased from Fluka. Other chemicals were Merck products. The two solvents, water and nitrobenzene, were mutually saturated. Nitrobenzene solution contained 50 mmol/L DMFC and 0.1 mol/L tetrabuthylammonium perchlorate (Bu_4NClO_4) as an organic electrolyte. For preparation of all aqueous solutions, redistilled water was used.

A graphite rod (black graphite), GrafTech, UCAR SNC, La Lechere France with a diameter of 0.113 cm has been used as a working electrode. Before modification with nitrobenzene solution, the surface of the electrode was polished on a SiC paper, treated in an ultrasonic bath for about 1 min in water, rinsed consequently with methanol, and dried on air. Thereafter, ca. 0.3 μL nitrobenzene solution was imposed on the electrode surface, while a thin film was formed by spontaneous spreading of the organic solution. An Ag/AgCl (saturated KCl) was the reference, while Pt wire served as an auxiliary electrode. Cyclic voltammetry (CV) and square-wave voltammetry (SWV) have been conducted by using μAUTOLAB III multipurpose potentiostat/galvanostat (Eco-Chemie, Utrecht, Netherlands).

Optical microscopy images were recorded with optical microscope DZ3 (Union, Japan) equipped with Suruga manipulator (1.5- to 70-fold magnification), connected to a video camera Sony 3CCD Exwave HAD.

AFM measurements were carried out with an atomic force microscope Dimension 3000 with an Extender Electronics Module from Veeco. The microscope was settled on an anti-vibration table in a closed box. The scans were made

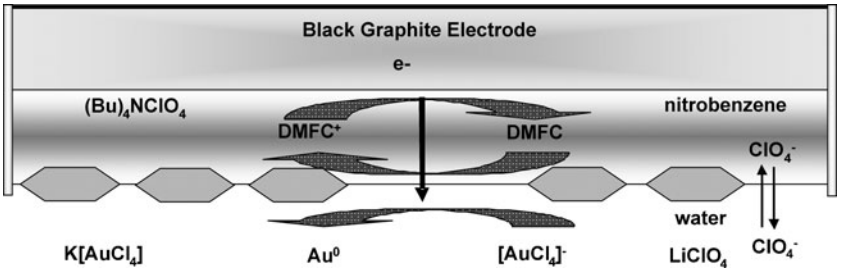

Fig. 1 Schematic representation of a thin organic film-modified electrode consisting of black graphite, modified with a thin film of nitrobenzene, containing DMFC as a redox probe and $(Bu)_4NClO_4$ as an organic electrolyte. The modified electrode is immersed into an aqueous electrolyte solution containing $LiClO_4$ as a supporting electrolyte and $K[AuCl_4]$ as an aqueous redox partner. The potential at the liquid interface is predominantly controlled by the partition of ClO_4^-

in tapping mode using *n*-doped Si-probe tips with 125-μm lengths, i.e., the *n*-doped Si-probe tip touched the surface of the sample, and several scans were performed on various spots. The drive frequency of the *n*-doped Si-probe tip was 315.1733 KHz, while the scan rate (time for measuring one line of the image) was 1 Hz. The images were scanned in topography, amplitude, and phase mode, with a resolution of 512×512 pixels. Rounded glass cover slips with a diameter of 25 and 0.17 mm thickness were used as substrates, at which the Au deposit was prepared following ex situ deposition protocol.

The SEM images were performed with Nova NanoLab 200 Dual Beam Microscope, a product of FEI (USA), using accelerating voltage of 10 kV (HV) and ETD as a detector. The energy dispersive X-ray spectroscopy spectra were recorded by using EDAX detector of AMETEK (USA), connected to the microscope. About 500 scans were accumulated to obtain the composition of the samples.

All experiments were performed at room temperature.

Results

Figure 2a shows representative cyclic voltammograms recorded with DMFC-modified thin-film electrode submerged in an aqueous electrolyte solution containing 0.1 mol/L $LiClO_4$. These voltammograms were recorded following an incubation of the thin-film electrode in a separate aqueous solution containing 1 mmol/L $K[AuCl_4]$ at different times in an ex situ deposition protocol. The main feature of the recorded voltammograms is the strong decreasing of the voltammetric response that is proportional to the incubation time. In addition, the peak potential separation increases slightly for deposition times from 0 to 400 s. For longer deposition times, the potential of the peak-to-peak separation is significantly enlarged. When the deposition time was longer than 900 s, the voltammetric response of the modified electrode virtually vanishes (curve 5 in Fig. 2a). Results collected from controlling experiments in which the film electrode was incubated in a water phase free of $K[AuCl_4]$, are summarized in Fig. 2b. Obviously, the decrease of the voltammetric response due to leaching of the redox probe of the thin film is insignificant, implying that the current decrease presented in voltammograms of Fig. 2a is due to the effect caused by an interfacial reaction of the organic redox probe DMFC(nb) with the $[AuCl_4]_{(w)}^-$ ions.

Shown in Fig. 3 are optical microscopy images of the gold metal deposit obtained at the w/nb interface. To get the snapshots on Fig. 3, we performed experiments on a glass support, where a droplet of the nitrobenzene solution (0.5 mL) containing DMFC has been brought into contact with a 1-mmol/L $K[AuCl_4]$ aqueous solution droplet of the same volume. Optical images have been recorded shortly thereafter. The spontaneous heterogeneous redox reaction between the DMFC(nb) and $[AuCl_4]^-$(w) resulted in formation of an Au deposit in a form of a wire at the w/nb interface. Under these conditions, the deposition process was quite rapid, resulting in a dense metal deposit rather than formation of Au nanoparticles. Yet, as implied by the AFM images of the adjacent region to the Au wire (Fig. 4a), the deposition starts by formation of about 100 nm clusters that gather together, and form a relatively compact film. The overall deposition process depends predominantly on the concentration ratio of the two redox counter-partners, i.e., $r=c(\text{DMFC(nb)})/c([AuCl_4]^-(w))$. The rate of the film formation and its density increases by decreasing the concentration ratio, i.e., by increasing the $[AuCl_4]^-$(w) concentration, at a constant concentration of DMFC(nb). As depicted in Fig. 4b, for $r=1$, no nanoparticles are visible and a swarm-like Au deposit was formed instead. In addition, Fig. 4c shows a SAM image of the same metal deposit. The presence of metallic Au was also confirmed by energy dispersive X-ray analysis, corresponding to the SEM image shown on Fig. 4c (data not shown).

Electrochemical (in situ) deposition was conducted by repetitive cycling of the potential under conditions of both CV and SWV, in an electrolyte solution of 0.1 mol/L $LiClO_4$ containing different concentrations of $[AuCl_4]^-$(w) ions. As

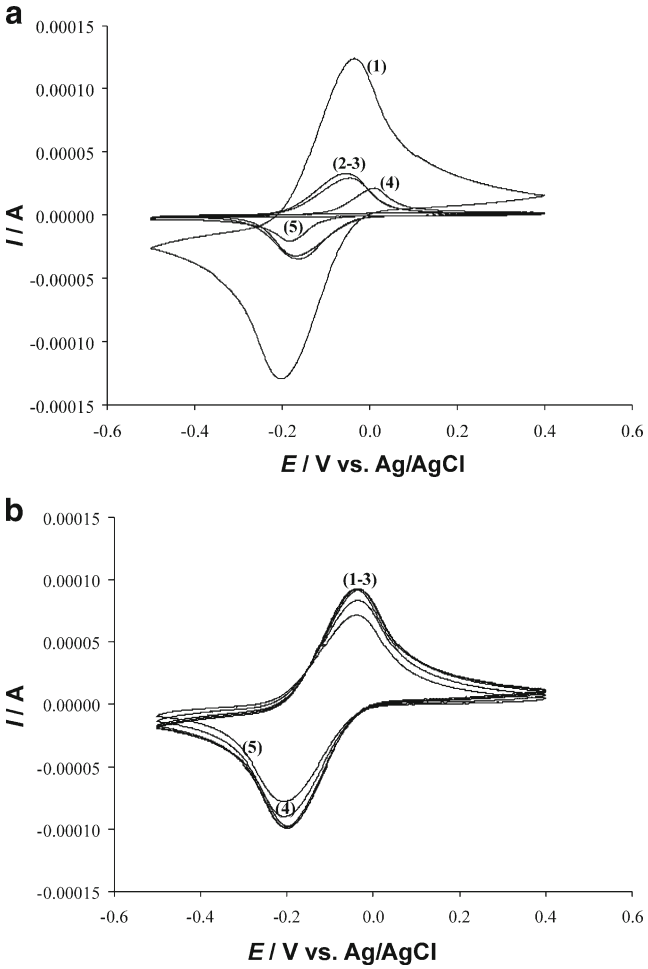

Fig. 2 Ex situ deposition protocol. **a** Cyclic voltammograms recorded with a modified thin film electrode in contact with a 0.1 mol/L $LiClO_4$ aqueous solution, following the incubation of the electrode in a separate aqueous solution containing 1 mmol/L $K[AuCl_4]$ for 0 (*1*), 45 (*2*), 200 (*3*), 600 (*4*), and 1,000 s (*5*). The scan rate was ν=50 mV/s. The nitrobenzene film contained 50 mmol/L of DMFC and 0.1 mol/L Bu_4NClO_4. Each voltammogram was recorded with a new modified electrode. **b** Controlled experiment performed under identical conditions as for (**a**), but the incubation solution was free of $K[AuCl_4]$ and contained only nitrobenzene saturated water

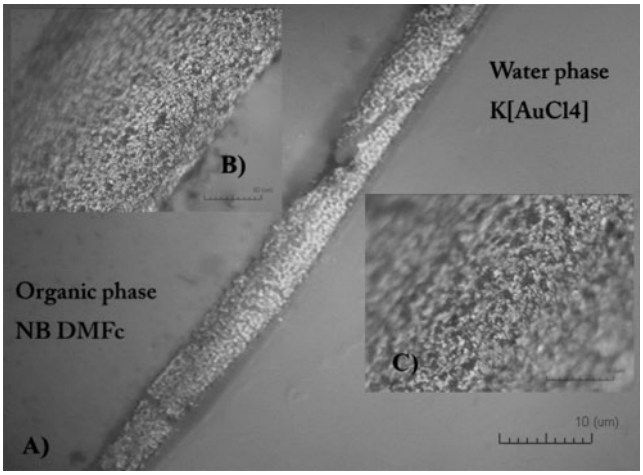

Fig. 3 **a** Optical microscopy image of a gold wire formed right after the contact of a water droplet containing 1 mmol/L $K[AuCl_4]$ and a nitrobenzene droplet containing 50 mmol/L DMFC and 0.1 mol/L Bu_4NClO_4. The magnification scale is 10 μm. Snapshots at figures (**b**) and (**c**) show the same metal deposit with bigger magnifications on a scale of 50 and 30 μm, respectively

can be seen from Fig. 5, a significant decrease of the current with the time of the potential cycling is observed, for both CV and SWV. After a certain critical deposition time, the diminishing of the voltammetric response ceases and a stable voltammetric response is obtained.

Shown in Fig. 6a is the dependence of the anodic peak current of the cyclic voltammograms ($I_{p,a}$) on the time of potential cycling for several different concentrations of $[AuCl_4]^-$(w) ions. Generally speaking, for all concentrations of $[AuCl_4]^-$(w) ions, the current decreases with time of the potential cycling. The rate of the current decrease is more significant at larger $[AuCl_4]^-$(w) concentrations. This is shown more precisely in Fig. 6b, where the ordinate displays the current variation rate $\nu=\Delta I_{p,a}/\Delta t$, where $\Delta I_{p,a}$ is the difference in the anodic peak current between two successive potential cycles, and Δt is the time elapsed between two sampling points (i.e., Δt is equal to the time of a single potential cycle).

Besides the concentration ratio of DMFC(nb) and $[AuCl_4]^-$(w) ions, the rate of Au deposition is expected to be dependent on the potential difference at the w/nb interface, defined as $\Delta_w^{nb}\phi = \phi_{nb} - \phi_w$, where ϕ is the symbol for the inner potential. In the present experimental arrangement, the potential difference $\Delta_w^{nb}\phi$ is predominantly controlled by the partition of common ClO_4^- ions, being present in a large excess compared to all other ionic species in the system. The deposition process was studied with SWV for three different concentrations of ClO_4^- (w), while keeping all other participants at a constant level. The results summarized in Fig. 7 show the net peak current decreases more rapidly by increasing the aqueous concentration of ClO_4^-(w), indicating acceleration of the gold deposition as the potential at the water side is becoming more positive.

In order to inspect the influence of the gold deposit to the kinetics of the overall electrochemical process at the modified electrodes, a series of experiments has been performed by varying the scan rate (in CV) and frequency of the potential modulation (in SWV experiments). Previously, the electrode was in situ modified with a gold deposit in a solution containing 100 μmol/L $[AuCl_4]^-$(w) until reaching a stable cyclic voltammetric response. In the absence of the Au deposit, peak potentials of both cathodic and anodic CV peaks are independent on the scan rate for $\nu \leq 300$ mV s^{-1} (data not shown). However, in the presence of the Au deposit, the peak potential separation increases in proportion

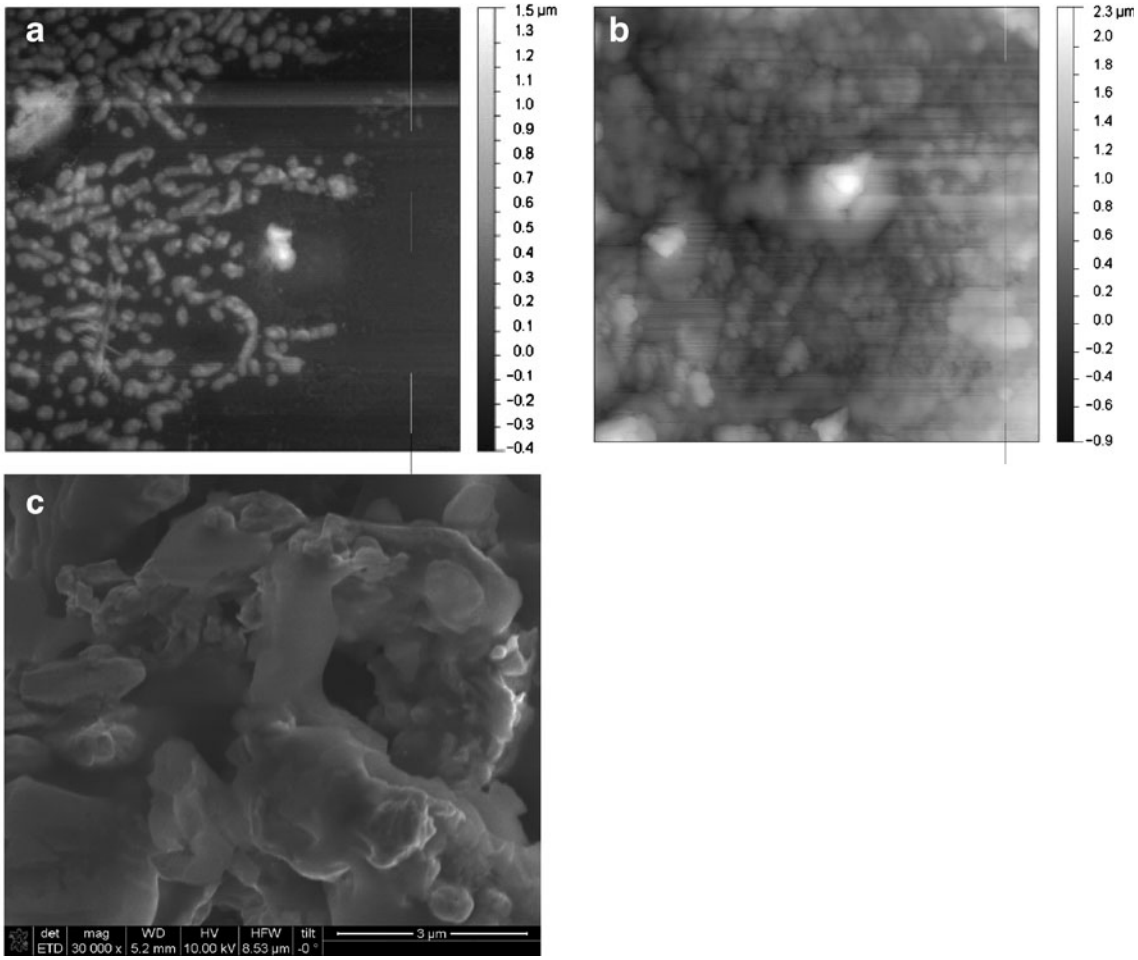

Fig. 4 AFM images of Au deposit obtained with an aqueous phase containing 1 mmol/L (**a**) and 50 mmol/L K[$AuCl_4$] (**b**). **c** SEM image of Au deposited obtained under the same conditions as for (**b**). The other conditions are the same as for Fig. 3

to the scan rate, even in the region of moderate scan rates ($5 \leq \nu/(\text{mV s}^{-1}) \leq 100$), as depicted in Fig. 8a. This implies that the Au deposit affects significantly the rate of the electrochemical process at the modified electrode.

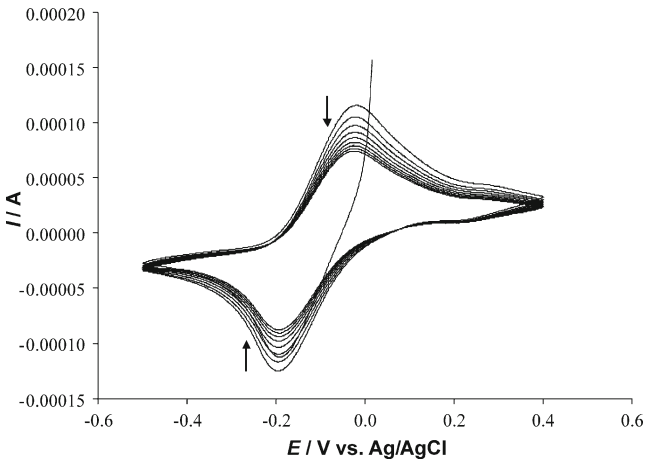

Fig. 5 In situ deposition protocol. Repetitive cyclic voltammograms recorded with a modified electrode in contact with a 0.1 mol/L $LiClO_4$ containing 100 µmol/L K[$AuCl_4$] at a scan rate of 50 mV/s. The other conditions are the same as for Fig. 2

The kinetic effects were also analyzed following the methodology of the quasireversible maximum in SWV [35, 36]. This requires inspection of the frequency normalized net peak current $\Delta I_p f^{-0.5}$ versus log (f). Within the quasireversible kinetic region, this dependence has a parabolic shape, with a maximum located at a critical frequency (f_{max}), which is proportional to the standard rate constant. Figure 8b compares the quasireversible maxima measured before (curve 1) and after modification of the w/nb interface with a gold deposit (curve 2). In the absence of the Au deposit, the critical frequency is f_{max}=25 Hz (curve 1 in Fig. 8b), whereas in the presence of the Au deposit, only the descending part of the quasireversible maximum was observed (curve 2 in Fig. 8b), revealing the maximum is positioned in a frequency range lower than 8 Hz, (i.e., the lowest available frequency with the used instrumentation). These results agree with the previous CV data, confirming that the gold deposit impedes significantly the rate of the electrochemical process at the modified electrode.

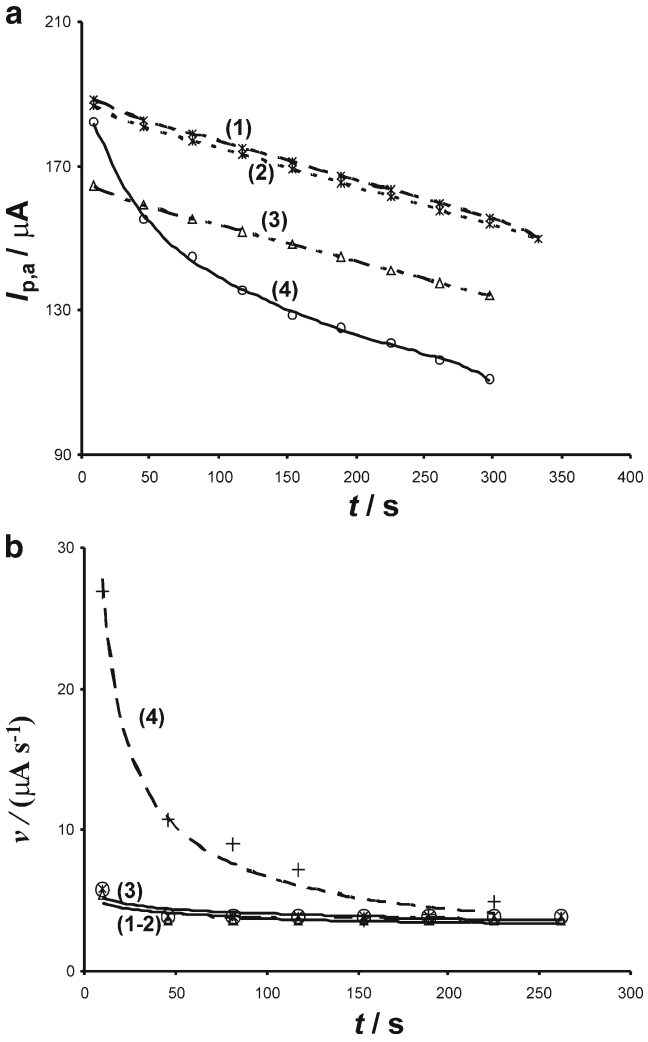

Fig. 6 Dependence of the CV anodic peak current ($I_{p,a}$) (**a**) and the current variation rate (v) (**b**) on the time of potential cycling. Concentrations of $[AuCl_4]^-$ ions were: 0.1 (*1*); 1 (*2*); 10 (*3*), and 100 μmol/L (*4*). (The rate of current variation is defined as $v=\Delta I_{p,a}/\Delta t$ where $\Delta I_{p,a}$ is the difference between two successive potential cycles; Δt is the time duration of a single potential cycle). The scan rate was 50 mV/s. The other conditions are the same as for Fig. 2

Once formed at the liquid interface, the gold deposit can act as an effective catalyst for electron transfer reactions between DMFC(nb) and redox reactants present in the aqueous phase. Figure 9 illustrates the catalytic effect of gold on the electron transfer reactions of DMFC(nb) with $[Fe(CN)_6]^{3-}$(w) and H_2O_2(w). Experiments are performed after saturation of the liquid interface with a gold deposit in the in situ deposition protocol. Thereafter, the gold-modified electrode was transferred in an $[AuCl_4]^-$(w)-free electrolyte solution containing either $[Fe(CN)_6]^{3-}$(w) or H_2O_2(w). In such scenario, it was observed that the response of the gold-modified thin film electrode is significantly higher than the corresponding response recorded in the absence of the gold deposit.

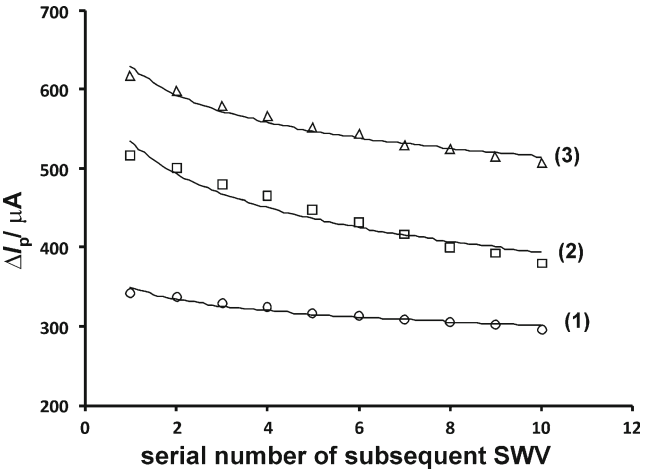

Fig. 7 Variation of the net SW peak current for ten subsequent SW voltammograms recorded in a $LiClO_4$(w) solution at concentration of 0.1 (*1*), 0.5 (*2*), and 1 mol/L (*3*). Concentration of $K[AuCl_4]$ was 100 μmol/L. The instrumental parameters were: frequency f=20 Hz, amplitude E_{sw}=50 mV, and potential step dE=1 mV. The other conditions are the same as for Fig. 2

Discussion

The overall electrochemical process at thin organic film-modified electrodes proceeds as a complex electron–ion coupled reaction (1). In the present system, the electrode reaction of the lipophilic redox compound DMFC (2) is accompanied by the concomitant transfer of charge-compensating ClO_4^- anions across the w/nb interface (3):

$$DMFC(nb) + ClO_4^-(w) \rightleftarrows DMFC^+(nb) + ClO_4^-(nb) + e^- \quad (1)$$

$$DMFC(nb) \rightleftarrows DMFC^+(nb) + e^- \quad (2)$$

$$ClO_4^-(w) \rightleftarrows ClO_4^-(nb) \quad (3)$$

As demonstrated in a series of previous studies [35, 36], the ion transfer reaction (3) is the rate-limiting step of the overall electrochemical process (1). This feature makes the system particularly sensitive to the nature of the liquid–liquid interface, which provides the basis for electrochemical monitoring of the metal deposit at this liquid border.

In the presence of $[AuCl_4]^-$(w), a spontaneous interfacial redox reaction with DMFC(nb) is taking place to produce metallic gold at the w/nb interface, as it is confirmed by the results presented in Figs. 3 and 4. Our results, as well as the findings of others [20], imply that the redox reaction is of heterogeneous nature, where the two redox partners exchange electrons across the liquid interface, while being embedded in different liquid phases. The overall process can be rationalized

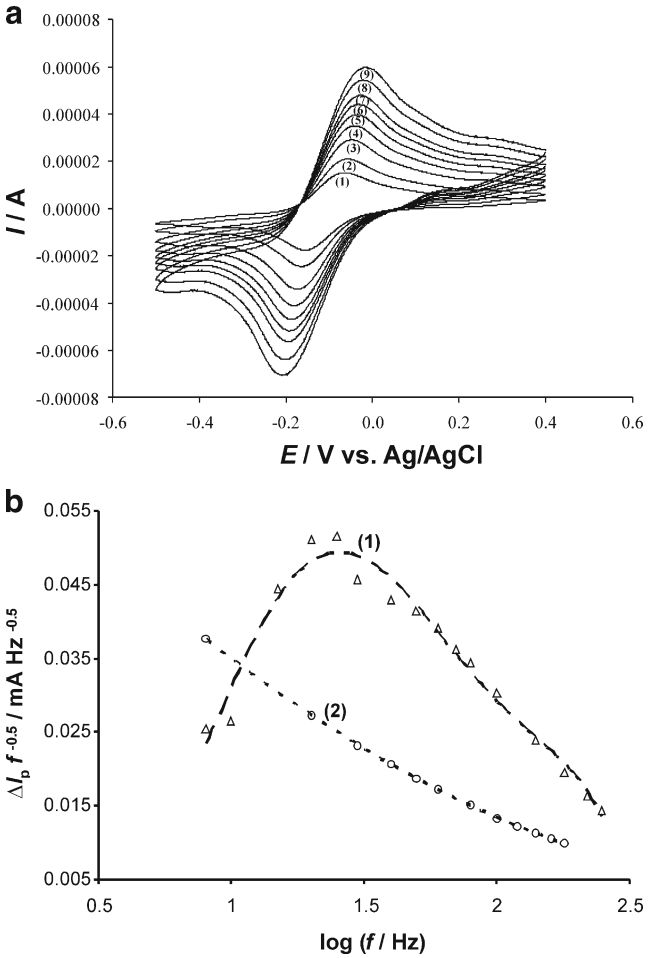

Fig. 8 **a** Effect of the scan rate to the cyclic voltammograms of an Au-modified thin organic film electrode. The scan rates were: 5 (*1*), 10 (*2*), 20 (*3*), 30 (*4*), 40 (*5*), 50 (*6*), 60 (*7*), 80 (*8*), and 100 mV/s (*9*). **b** Quasireversible maxima recorded with a thin-film electrode (*1*) and Au-modified thin film electrode followed controlled potential deposition procedure (*2*) in contact with a 0.1 mol/L $LiClO_4$ aqueous electrolyte solution. The NB film contained 50 mmol/L DMFC and 0.1 mol/L Bu_4NClO_4. In all cases, the gold deposition was conducted under in situ protocol by a potential cycling in 0.1 mol/L $LiClO_4$ containing 100 μmol/L $[AuCl_4]^-$(w) until reaching a constant voltammetric response

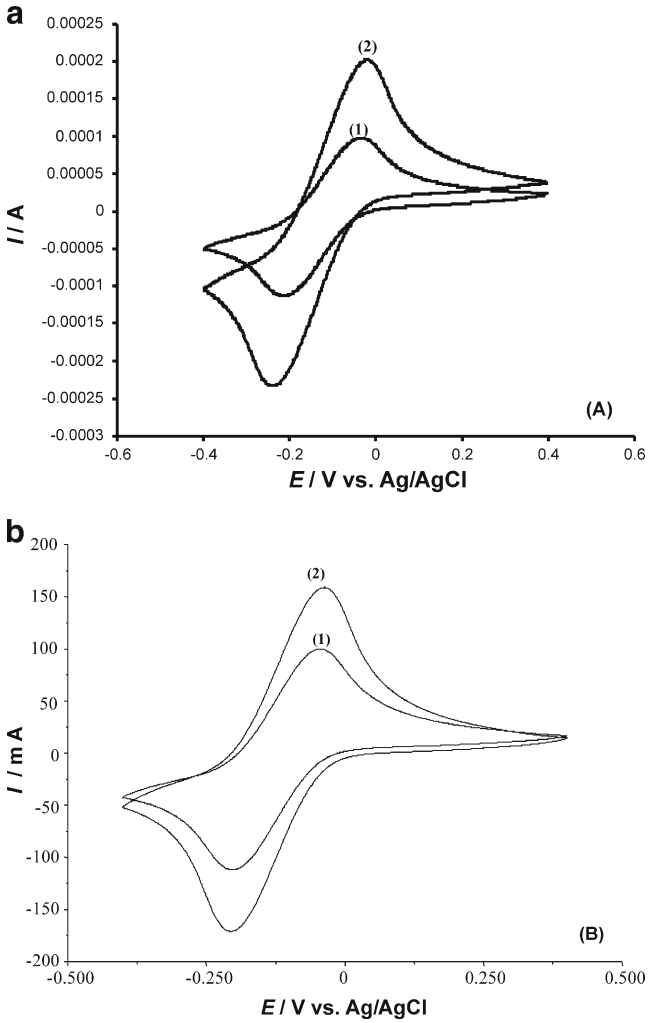

Fig. 9 Catalytic effect of the gold deposit (*curves 1*) on the interfacial electron transfer reaction between DMFC(nb) and 1 mM $[Fe(CN)_6]^{3-}$(w) (**a**) and 10 mM H_2O_2(w) (**b**). Curves *2* correspond to the experiments in the absence of gold particles. The electrode was modified with a gold deposit according to the "in situ" deposition protocol in 0.1 mol/L $LiClO_4$(w) containing 0.17 mmol/L $[AuCl_4]^-$(w) until reaching a stable voltammetric response. The other conditions are the same as for Fig. 2

with Eq. 4. Even though, from a mechanistic point of view the process is certainly much more complicated.

$$3\mathrm{DMFC(nb)} + [\mathrm{AuCl_4}]^-(\mathrm{w}) + 3\mathrm{ClO_4}^-(\mathrm{w}) \rightleftarrows \mathrm{Au(s)} + 3\mathrm{DMFC}^+(\mathrm{nb}) + 4\mathrm{Cl}^-(\mathrm{w}) + 3\mathrm{ClO_4}^-(\mathrm{nb}) \quad (4)$$

The latter reaction holds true, at least, for the commencement of the heterogeneous redox reaction at the liquid interface. Thereafter, as soon as clusters of gold deposit are formed at the liquid interface, they could act as kind of bipolar electrodes, thus conducting the electron transfers between DMFC(nb) and $[AuCl_4]^-$(w). In such scenario, the rate of reaction might not depend any longer on the electron transfer rate across the liquid interface (reaction 4), and it can be controlled by the rate of the electron exchange of either DMFC(nb) or $[AuCl_4]^-$(w) at the gold clusters. Moreover, $[AuCl_4]^-$(w) ions might be a subject of hydrolysis in the aqueous phase, and several other complex ionic species, with distinct redox potentials, can participate in the redox reaction with DMFC(nb). As pointed out in [39], the hydrolysis of $[AuCl_4]^-$(w) is neglegible in concentrated hydrochloride media. However, under such conditions, the instability of $DMFC^+$(nb) is very probable, which was the reason for avoiding such medium in our experiments.

The main thermodynamic driving force for the metal deposition depends on the difference between the standard

redox potentials of the two redox couples, DMFC(nb)/$DMFC^+$(nb) (E^{θ}=0.406 V vs. SHE) and $[AuCl_4]^-$(w)/Au (s) (E^{θ}=1.002 V vs. SHE), as well as the concentration ratio of the redox partners, as predicted by the Nernst Eq. 5

$$\Delta_w^{nb}\phi = E^{\ominus}_{DMFC^+(nb)/DMFC(nb)} - E^{\ominus}_{[AuCl_4](w)/Au(s)} + \frac{RT}{3F} \times \ln \frac{a^3_{DMFC(nb)} a_{[AuCl_4]^-(w)} a^3_{ClO_4^-(w)}}{a^3_{DMFC^+(nb)} a^4_{Cl^-(w)} a^3_{ClO_4^-(nb)}} \quad (5)$$

In the ex situ deposition protocol, the rate of the heterogeneous reaction (4) depends predominantly on the concentration of the redox partners. The ultimate amount of the metal deposit is determined by the limiting reactant, i.e., the reactant that is exhausted in the course of the reaction. Most frequently that is the DMFC(nb) (e.g., Fig. 2a). Both concentration of the redox partners and deposition time affect the morphology of the metal deposit. Microscopic images shown on Figs. 3 and 4 indicate the deposition process commences by formation of nanometer gold clusters (Fig. 4a) that gather together with time, thus forming a swarm-like metal deposit (Fig. 3). As indicated by the voltammetric data shown in Fig. 2a, the metal deposit is mainly confined to the liquid interface, blocking the active surface area for the ion transfer reaction. This phenomenon produces a decrease of the voltammetric response. However, under prolonged deposition time, the density of the metal deposit increases, hindering the rate of the ion transfer reaction. This effect is manifested by the enlargement of the CV peak potential separation (curves 3 and 4 in Fig. 2a). At sufficiently long deposition time (curve 5 in Fig. 2a), the metal film can block completely the ion transfer reaction that results in vanishing of the voltammetric response of the modified electrode.

More appealing is the in situ electrochemical deposition protocol. In this scenario, the reactant DMFC(nb) is being electrochemically regenerated at the electrode surface in the course of the redox reaction (4), by performing a permanent cycling of the electrode potential. The redox couple DMFC (nb)/$DMFC^+$(nb) acts as an electron shuttle from the electrode to the liquid interface to enable electrochemical deposition of gold. With the electrode potential cycling, the concentration of DMFC(nb) and $DMFC^+$(nb) in the thin film is controlled, fluctuating periodically as dictated by the electrode reaction (2), which affects the rate of reaction (4). Moreover, the extent of the reaction is not limited by the exhaustion of the thin film with the redox reactant, enabling the deposition process to proceed further and to be controlled electrochemically.

The gold deposit blocks partially the liquid interface, causing the diminishing of the voltammetric response with time in both CV (Fig. 5) and SWV (data not shown). This effect is similar to the one observed under ex situ deposition protocol. Interestingly, the net SW peak potential and the CV peak potential separation do not vary notably, revealing that the rate of the ion transfer reaction (3) is not affected as significantly as in the ex situ deposition. As can be inferred from the results presented in Fig. 6a, the amount of the gold deposit is proportional to the time of the deposition and the concentration of the redox partners. More specifically, Fig. 6b shows that the rate of metal deposit decreases exponentially with time, while being strongly sensitive to the concentration of the redox partners. Interestingly, after sufficiently long deposition time, the rate of metal deposition is reaching a constant value, regardless the concentration of the redox partners (the lower linear region of all curves in Fig. 6b). Under such conditions, constant and stable voltammograms were obtained, without detecting any complete blocking of the liquid–liquid interface by the metal deposit. Obviously, the metal deposit obtained during in situ deposition is attributed with a morphology that allows the transfer of ions, which is opposite to the ex situ obtained deposit (compare curve 5 in Fig. 2a with the last curve in both Fig. 5).

At this point it is particularly important to emphasize that the in situ deposition is conducted under permanent transfer of anions across the liquid interface due to overall reaction (1). Besides, the ion transfer reaction is indispensable for the heterogeneous redox reaction (4) as well, as it maintains the charge neutrality of both liquid phases. Furthermore, the presence of the common ClO_4^- ions in both liquid phases in a large excess has a task to control the potential difference across the liquid interface, which is defined according to the following form of the Nernst equation:

$$\Delta_w^{nb}\phi = \Delta_w^{nb}\phi^{\ominus}_{ClO_4^-} + \frac{RT}{F} \ln \frac{a_{ClO_4^-(nb)}}{a_{ClO_4^-(w)}} \quad (6)$$

As follows from Eq. 6, increasing the concentration of ClO_4^-(w) makes the inner potential in the organic phase more negative relative to the aqueous phase, causing acceleration of the electron transfer from the organic to the aqueous phase, which explains the data presented in Fig. 7. This analysis corroborates the assumption that the redox reaction at the liquid interface is of heterogeneous nature, where the two reactants are embedded in different phases involving electron transfer across the liquid interface.

Although the blocking of the liquid–liquid interface was not observed during the in situ deposition protocol, yet the presence of gold deposit hinders the rate of ion transfer, as clearly evidenced by both cyclic (Fig. 8a) and SW voltammetry (Fig. 8b). On the other hand, the gold particles are an effective catalyst for the electron transfer reactions at the liquid interface, as illustrated by the results in Fig. 9. Although the exact mechanism of the catalytic effect cannot be easily revealed, we assume that the gold clusters act as bipolar electrodes wiring and accelerating the electron transfer across the liquid interface.

Conclusion

We report in this work on two different protocols to form metallic gold at a liquid–liquid interface. The gold deposit is formed via an interfacial electron exchange between two redox compounds present in conjoined immiscible liquid phases. The structure of the Au deposit depends on various factors such as the concentration ratio of both redox counter-partners, the contacting time of liquid phases, while the interfacial potential difference also plays significant role. The structure and the features of the gold deposited at the liquid–liquid interface are significantly affected by the deposition protocol. In the so-called ex situ approach, the two liquid phases with redox counter-partners dissolved in them are left to exchange electrons without applying potential from an outside source. This scenario leads to formation of a gold deposit that hinders the ion-transfer reaction across the liquid–liquid interface, as detected by the voltammetry at thin organic film-modified electrode. In the second in situ approach, an Au deposit is also formed, which shows less pronounced ion transfer hindering effect. In both scenarios, we could detect that gold nanoparticles display catalytic effects by enhancing the interfacial electron transfer reactions between the DMFC and redox substrates dissolved in the water phase. Both protocols for obtaining Au deposit at the liquid–liquid interface are simple and easily scalable. Both methods allow facile tuning of the thickness of the metallic gold. Additional studies should reveal the catalytic effects of the interfacial Au nanodeposit towards various relevant biomolecules such as DNA, coenzymes, and water soluble vitamins, which is the next task in our lab.

Acknowledgment The authors take the opportunity to acknowledge gratefully the DAAD (Deutscher Akademirscher Austausch Dienst) bilateral project in the frame of Stability Pact for South Eastern Europe, sponsored by FR Germany. Also authors acknowledge gratefully Dr. Winfried Böhlmann and B.Sc. Francis Bern from the University of Leipzig, Faculty of Physics and Earth Sciences for the recording of the images with optical microscopy, atomic force microscopy, and scan electron microscopy.

References

1. Lahtinen R, Jensen H, Fermin DJ (2003) In: Volkov AG (ed) Interfacial catalysis. Marcel Dekker, New York, p 611
2. Kimling J, Maier M, Okenve B, Kotaidis V, Ballot H, Plech A (2006) J Phys Chem B 110:15700–15707
3. Zhang J, Langille MR, Mirkin CA (2011) Nano Lett 11:2495–2498
4. Swami A, Kumar A, D'Costa M, Pasricha R, Sastry M (2004) J Mater Chem 14:2696–2702
5. Gu H, Yang Z, Gao J, Chang CK, Xu B (2005) J Am Chem Soc 127:34–35
6. Knake R, Fahmi AW, Tofail SAT, Cohessy J, Mihov M, Cinnane VJ (2005) Langmuir 21:1001–1008
7. Reetz MT, Helbig W (1994) J Am Chem Soc 116:7401–7402
8. Dai LL, Sharma R, Wu C-Y (2005) Langmuir 21:26–41
9. Su B, Abid J-P, Fermin DJ, Girault HH, Hofmannová H, Krtil P, Samec Z (2004) J Am Chem Soc 126:915–919
10. Lin Y, Böker A, Skaff H, Cookson D, Dinsmore AD, Emrick T, Russell TP (2005) Langmuir 21:191–194
11. Yogev D, Efrima S (1988) J Phys Chem B 92:5754–5760
12. Kumar D, Mandal S, Mathew SP, Selvakannan PR, Mandale AB, Chaudhari RV, Sastry M (2002) Langmuir 18:6478–6483
13. Dryfe RAW, Simm AO, Kralj B (2003) J Am Chem Soc 125:13014–13015
14. Zheng L, Li J (2005) J Phys Chem B 109:1108–1112
15. Sakata JK, Dwoskin AD, Vogorita JL, Spain EM (2005) J Phys Chem B 109:138–141
16. Scholz F, Hasse U (2005) Electrochem Commun 7:541–546
17. Campbell AI, Dryfe RA, Haw MD (2009) Anal Sci 25(2):307–310
18. Dryfe RAW (2006) Phys Chem Chem Phys 8:1869–1883
19. Guainazzi M, Silvestri G, Serravalle G (1975) Chem Commun 6:200–201
20. Cheng YF, Schiffrin DJ (1996) J Chem Soc Faraday Trans 92:3865–3871
21. Johans CRC, Kontturi K, Schiffrin DJ (2002) J Electroanal Chem 526:29–35
22. Johans C, Liljeroth P, Kontturi K (2002) Phys Chem Chem Phys 4:1067–1071
23. Johans C, Lahtinen R, Kontturi K, Schiffrin DJ (2000) J Electroanal Chem 488:99–109
24. Platt M, Dryfe RAW, Roberts EPL (2004) Electrochim Acta 49:3937–3945
25. Platt M, Dryfe RAW (2007) J Electroanal Chem 599:323–332
26. Trojánek A, Langmaier J, Samec Z (2007) J Electroanal Chem 599:160–166
27. Johans C, Clohessy J, Fantini S, Kontturi K, Cunnane VJ (2002) Electrochem Commun 4:227–230
28. Hasse U, Palm GJ, Hinrichs W, Schäfer J, Scholz F (2011) Phys Chem Chem Phys 13:12254–12260
29. Mirčeski V (2006) Electrochem Commun 8:123–128
30. Mirčeski V, Gulaboski R (2006) J Phys Chem B 110:2812–2820
31. Song J, Shin H, Kang C (2008) Bul Korean Chem Soc 29:1983–1987
32. Sholz F, Komorsky-Lovrić Š, Lovrić M (2000) Electrochem Commun 2:112–118
33. Komorsky-Lovrić Š, Riedl K, Gulaboski R, Mirčeski V, Scholz F (2002) Langmuir 18:8000–8005
34. Scholz F, Schröder U, Gulaboski R (2005) Electrochemistry of immobilized particles and droplets. Springer, Heidelberg
35. Quentel F, Mirčeski V, L'Her M (2005) Anal Chem 77:1940–1949
36. Mirčeski V, Quentel F, L'Her M, Pondaven A (2005) Electrochem Commun 7:1122–1128
37. Shi C, Anson FC (1999) J Phys Chem B 103:6283–6289
38. Mirčeski V, Quentel F, L'Her M, Elleouet C (2007) J Phys Chem C 111:8283–8290
39. Almgren L (1971) Acta Chimica Scandinavica 25:3713–3720